Design of a Planar Cable-Driven Parallel Crane without Parasitic Tilt

Lionel Étienne, Philippe Cardou, Marceau Métillon, Stéphane Caro

▶ **To cite this version:**

Lionel Étienne, Philippe Cardou, Marceau Métillon, Stéphane Caro. Design of a Planar Cable-Driven Parallel Crane without Parasitic Tilt. Journal of Mechanisms and Robotics, 2022, 14 (4), 10.1115/1.4054081 . hal-03758211

HAL Id: hal-03758211
https://hal.science/hal-03758211

Submitted on 23 Aug 2022

HAL is a multi-disciplinary open access archive for the deposit and dissemination of scientific research documents, whether they are published or not. The documents may come from teaching and research institutions in France or abroad, or from public or private research centers.

L'archive ouverte pluridisciplinaire **HAL**, est destinée au dépôt et à la diffusion de documents scientifiques de niveau recherche, publiés ou non, émanant des établissements d'enseignement et de recherche français ou étrangers, des laboratoires publics ou privés.

Design of a Planar Cable-Driven Parallel Crane without Parasitic Tilt

Lionel Étienne[1,2], **Philippe Cardou**[3]*, **Marceau Métillon**[1,2], **Stéphane Caro**[1,2]

[1] Laboratoire des Sciences du Numérique de Nantes (LS2N), UMR CNRS 6004, 44300 Nantes, France

[2] Centre National de la Recherche Scientifique (CNRS), 44321 Nantes, France

[3] Laboratoire de robotique, Département de génie mécanique, Université Laval, Québec, QC, Canada

Emails: lioetienne@laposte.net, pcardou@gmc.ulaval.ca,

marceau.metillon@ls2n.fr, stephane.caro@ls2n.fr

ABSTRACT

Cable-Driven Parallel Robots (CDPRs) offer high payload capacities, large translational workspace and high dynamics performances. Their rotational workspace is generally far more limited, however, which can be resolved by using cable loops, as was shown in previous research. In the case of fully-constrained CDPRs, cable loops can induce unwanted torques on the moving-platform, causing it to tilt and move away from its intended position, which we call parasitic tilt. Hence, the orientation accuracy of such robots is usually limited. This paper deals with the design, modelling and prototyping of a planar CDPR with infinite rotations, without parasitic tilt and without an additional motor. This robot, which we call a Cable-Driven Parallel Crane (CDPC), is composed of a mobile platform (MP) with an embedded mechanism and a transmission module. The MP is linked to the frame by four cables, three of them acting in parallel, forming in effect a double parallelogram. Among these three parallel cables, two form a cable loop, i.e., they are two strands of the same cable redirected to and from the MP through an embedded pulley. The two-degree-of-freedom (dof) motions of the moving-platform of the CDPC and

*Address all correspondence to this author.

the internal dof of its embedded mechanism are driven by a total of three actuators, which are fixed to the frame. As a consequence, the overall system is fully-actuated, its total mass and inertia in motion is reduced and it is free of parasitic tilts.

1 Introduction

CDPRs belong to a particular class of parallel robots where a moving-platform (MP) is linked to a base frame using cables. Motors are mounted on a rigid base frame and drive winches. The cables coiled on these winches are routed through exit points located on the rigid frame to anchor points on the moving-platform. The MP pose (position and orientation) is determined by controlling the cable lengths. CDPRs hold several advantages over classical parallel robots. They are inexpensive and can cover large workspaces [1]. The lightweight cables contribute to the lower inertia of the moving-platform and consequently to a better dynamic performance over classical parallel robots [2]. Another characteristic of CDPRs is their reconfigurability. Changing the overall geometry of the robot can be done by changing the positions of its exit points and anchor points. Reconfigurability of the CDPRs is suitable for versatile applications especially in an industrial context [3, 4, 5]. CDPRs have drawn researchers' interests towards robotic applications such as pick-and-place operations, robotic machining, manipulation, intralogistics measurements and calibration systems [6, 7, 8, 9]. Cable-Driven Parallel Cranes (CDPCs) can offer extremely large two-degree of freedom translational workspace. One cannot write the same of their rotational workspace, which is generally limited both by cable interferences [10, 11] and by bounds on their tensions. Several researchers have proposed solutions to this problem. Pott and Miermeister [12, 13] have proposed to resolve this problem by replacing a rigid moving-platform with an articulated dyad driven through nine or even twelve cables and by as many motors. Fortin-Côté et al. [14], also opted for replacing the MP with an articulated dyad in order to generate unlimited rotations, but they resorted to a cable loop circulating on an embedded pulley to drive this added rotation. This allowed them to reduce the number of cables and motors to seven, thereby reducing cost, complexity and the likelihood of interference. Liu et al. [15] and Khakpour et al. [16, 17, 18] had previously developed the idea of using cable loops in CDPRs, but for the purpose of extending their translational workspaces, not their rotational workspaces. Pursuing large rotational workspaces while keeping the number of motors and cables to a minimum, Lessanibahri et al. [19] proposed a simple fully-constrained CDPR crane with three degrees of freedom. This design uses as many motors and cables as it had degrees of freedom, making it simpler than those reported by either Pott and Miermeister [13] or Fortin-Côté et al. [14]. It comes with one

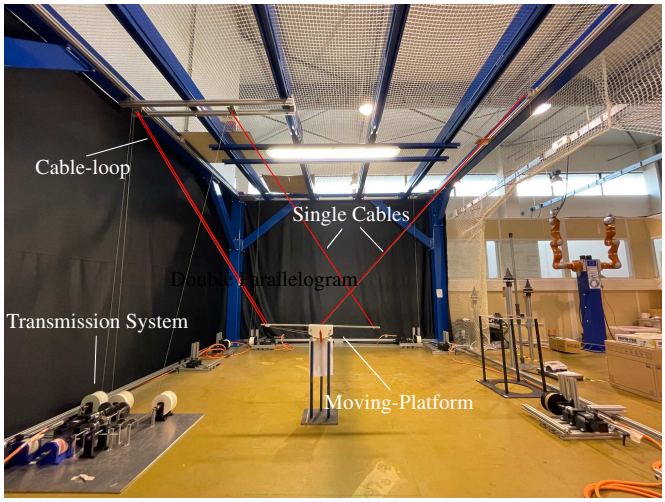

Fig. 1: CDPC with its double parallelogram and cable-loop

important drawback, however: any torque applied through the cable loop to the embedded pulley driving the dyad tilts the moving-platform. This drawback is due to the fully-constrained nature of this CDPR, by which it relies on gravity to keep its posture. In contrast, the overconstrained designs [13, 14] are not susceptible to this problem.

In this paper, we aim at fixing this problem, i.e., at making the moving-platform orientation independent from the torques applied by the cable loop while using no more motors than the number of degrees of freedom of the CDPR. To this end, we present the concept of a planar CDPC composed of a MP with an embedded mechanism and a transmission module, all of which are described in Section 2. The MP is linked to the frame through a double parallelogram—i.e., three parallel cables—which constrain its orientation, and include a cable-loop to actuate its embedded mechanism. A fourth cable is used to connect the MP to the frame and obtain a large translational workspace. The design and manufacturing of a transmission system is also described. Its aim is to control both the length of the double parallelogram and the cable-loop circulation, the latter being used to actuate the embedded mechanism onto the MP. This solution provides the robotic system with three inputs (three motors) and three outputs (three dof). The mathematical relationships between these inputs and outputs are derived in Section 3. In Section 4, the input-output relationships are used to determine the CDPC workspace and how it is influenced by some of the main design parameters. A prototype of the robot and an experimental validation are presented in Section 5. The results from these trials are discussed in Section 6 and conclusions are drawn in Section 7. Let us begin with a description of the proposed robot in the following section.

2 Robot Architecture

The photograph of Fig. 1 presents the proposed manipulator. Its architecture consists of a moving-platform (MP) and four cables, three of them forming a double parallelogram. This double parallelogram includes a cable loop used to drive the mechanism embedded on the MP. The rotations of the MP itself in the working plane are constrained by the double parallelogram [20] shown in Fig. 1. The transmission system is located in the lower-left corner of Fig. 1, while the cable exit points structure appear in the upper-left corner of the frame.

Figure 2 shows a simplified schematic of the proposed robot. The actuation system encompasses the left part of the mechanism, which includes winches 1, 2 and 3 driven by motors A and B through a transmission mechanism, and the right part, which includes winch 4 directly driven by motor C. Attached to the frame ceiling, the exit points A_1, A_2, A_3 and A_4 guide the four cables to the anchor points B_1, B_2, B_3 and B_4. The distances between the exit point A_i and the anchor point B_i is the cable length l_i, $i = 1,\ldots,4$. The unit vectors $\mathbf{u}_i$, $i = 1,\ldots,4$, are the directions of the corresponding cables.

The cable-loop parallelogram $A_2A_3B_3B_2$ drives a pulley of radius r_p and can be modelled as a single cable. The latter is named $A_{32}B_{32}$ and is shown in dotted line in Figure 2. Its direction is along unit vector $\mathbf{u}_{32}$ and its length is l_{32}. The distances between A_1 and A_{32} and B_1 and B_{32} must be the same to preserve the geometry of the double parallelogram $A_1A_{32}B_{32}B_1$. $\mathcal{F}_b$ is the fixed frame and $\mathcal{F}_p$ is the frame attached to the MP.

2.1 Cable-Loop Principle

As explained in [21, 22] and shown in Fig. 3, the cable-loop consists of a single cable. Both of its ends are coiled on separate winches, which in turn, are actuated by two motors. Eyelets are used to maintain constant exit-points, namely, A_2, A_3, and anchor-points, namely, B_2, B_3. The cable-loop is coiled around a pulley on the moving-platform. This pulley then acquires one rotational degree of freedom (dof) with respect to the moving-platform, which is used either to actuate a tool or to control additional degrees of freedom such as rotations over wide ranges. The purpose of the cable-loop is twofold. First, it aims at translating the moving platform when the coiling speeds of both motors have the same magnitude and direction. Second, it aims at rotating the embedded pulley by circulating the cable when both motors have the same coiling speeds, but in opposite directions.

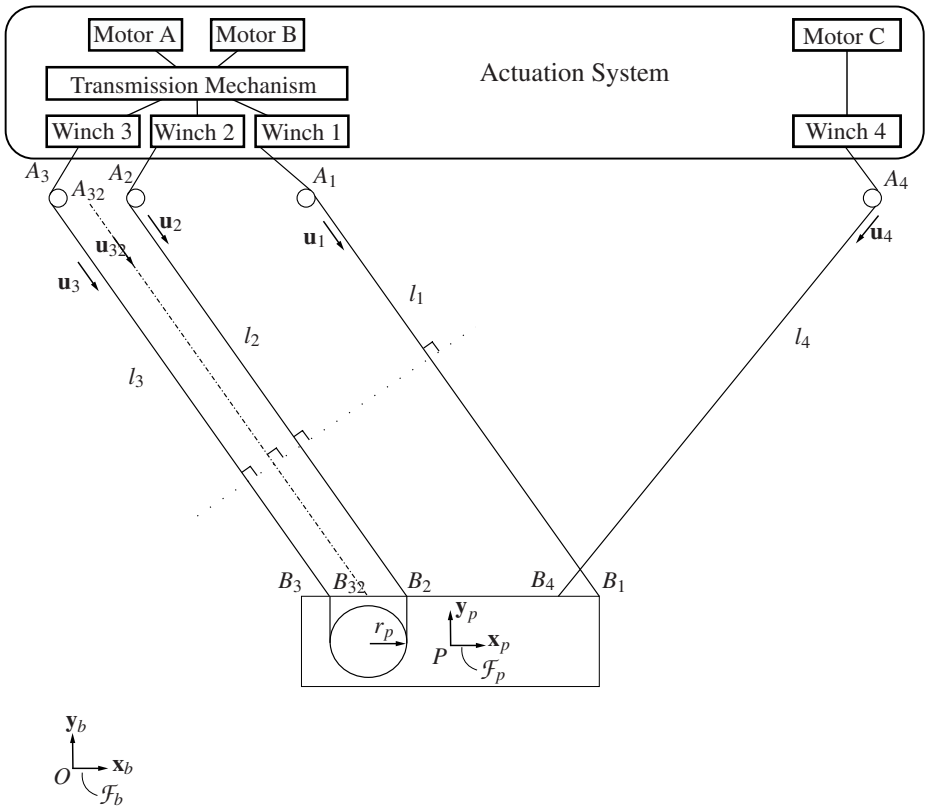

Fig. 2: Simplified concept scheme of the overall mechanism

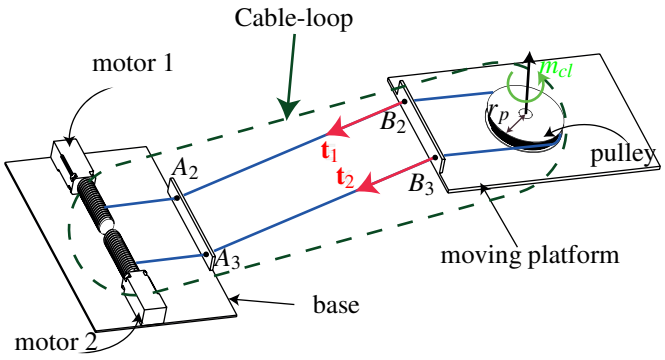

Fig. 3: Representation of a cable-loop [23]

2.2 Transmission System

The transmission system is described in Fig. 4. To control the added cable without an additional motor, the new cable has to follow the cable-loop elongation without being affected by its circulation. The solution proposed in this article is to use a differential mechanism knowing that the coiling speed of the added cable—here, cable 1—is then the mean of those of cables 2 and 3.

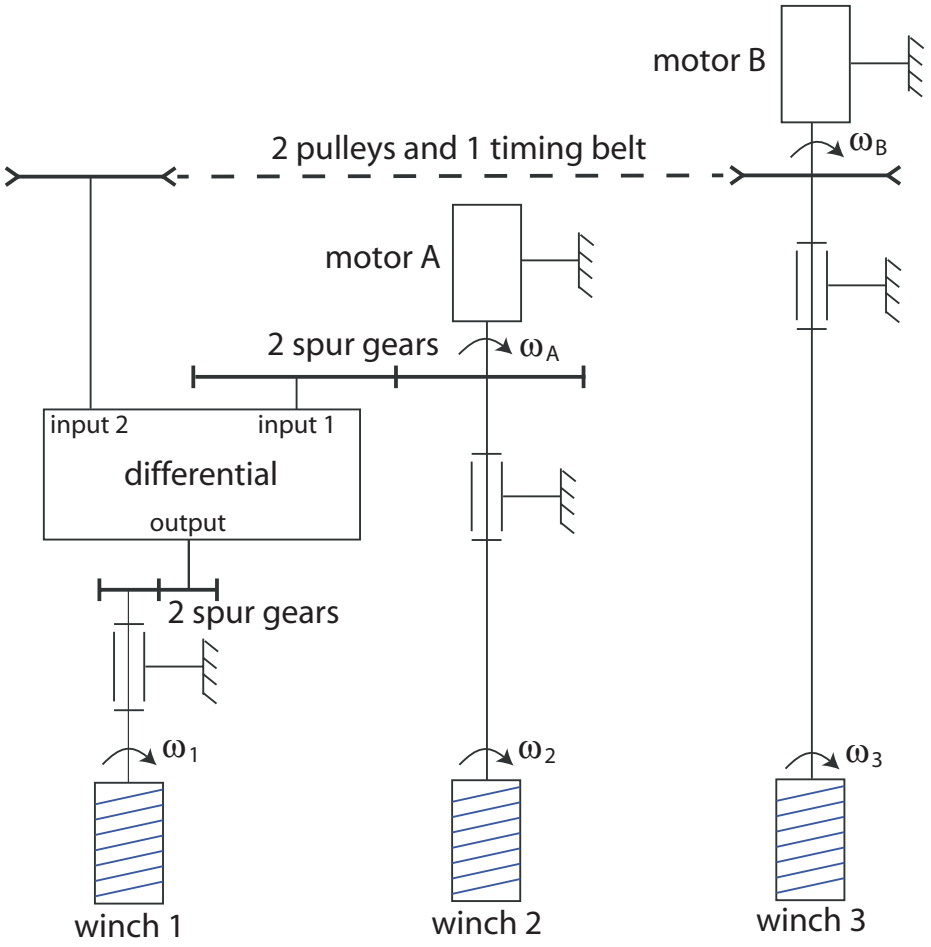

Fig. 4: Transmission system scheme

The two motors A and B directly drive the winches 2 and 3, and indirectly the winch 1 using a differential mechanism. The motor A actuates the latter through a gear and the motor B through a timing belt. The output of the differential drives the shaft 1 through a belt, in order to make the distance between them modular, and a gear to invert the direction of rotation.

The rotation velocities of the three motors ω_A ω_B and ω_C are defined in vector $\omega_{\mathbf{M}}$. The rotation velocities of the winches ω_1, ω_2, ω_3 and ω_4 are defined in vector $\omega_{\mathbf{E}}$. All the gear and timing pulley ratios of the transmission system are 1:1.

2.3 Parameterization

Robot modelling is segmented into four spaces : Cartesian space, cable-length space, winch space and joint space, as shown in Fig. 5. θ_A, θ_B and θ_C are the motor position angles, θ_i, $i = 1,\ldots,4$, are the winch position angles, l_i, $i = 1,\ldots,4$, are the cable lengths, and x, z, ϕ, α are the Cartesian parameters. More specifically, x and z are the absolute coordinates of the moving-platform, α is the cable-loop pulley position angle, and ϕ is the tilt angle of the moving-platform. In this paper,

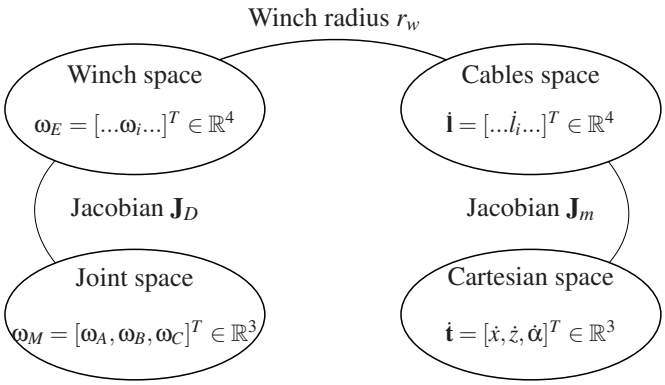

Fig. 5: Joint, wrench, cable and Cartesian velocity spaces of the robot

the double parallelogram guarantees $\phi = 0^\circ$ under the assumption that the cables are inextensible and always in tension. Having qualitatively described the functioning of the proposed CDPC, let us turn our attention to the mathematical equations representing its behavior in quasi-static conditions.

3 Kinetostatic Modelling

This section presents the kinetostatic modelling of the robot. In order to cover all the spaces defined in Subsection 2.3, let us start from the joint space. Thence, we can move successively to the winch space, the cable space and the Cartesian space.

3.1 Transmission Modelling

The transmission system is the link between the joint space and the winch space, as shown in Fig. 5. The arrays of motor and winch angular velocities are respectively called ω_M and ω_E, i.e.,

$$\omega_M = \begin{bmatrix} \omega_A \\ \omega_B \\ \omega_C \end{bmatrix} \text{ and } \omega_E = \begin{bmatrix} \omega_1 \\ \omega_2 \\ \omega_3 \\ \omega_4 \end{bmatrix} \tag{1}$$

The motors A, B and C directly drive the winches 2, 3 and 4,

$$\omega_2 = \omega_A \tag{2}$$

$$\omega_3 = \omega_B \tag{3}$$

$$\omega_4 = \omega_C \tag{4}$$

From Sec. 2.2, the output angular velocity of a differential is the mean of its two input angular velocities. Therefore, as motors A and B are linked to winch 1 through the differential, the relationship between the angular velocities ω_1, ω_2 and ω_3 of the three winches is defined as follows:

$$\omega_1 = \frac{\omega_2 + \omega_3}{2}. \tag{5}$$

Thus, Eqs. (6) and (7) describe the Jacobian $\mathbf{J}_D$, which maps the winch angular velocities ω_E onto the motor angular velocities ω_M:

$$\mathbf{J}_D = \begin{bmatrix} \frac{1}{2} & \frac{1}{2} & 0 \\ 1 & 0 & 0 \\ 0 & 1 & 0 \\ 0 & 0 & 1 \end{bmatrix}, \tag{6}$$

$$\omega_E = \mathbf{J}_D \, \omega_M. \tag{7}$$

It is a simple matter to note that the uncoiling speed $\dot{l}_i$ of the i^{th} cable is related to the corresponding winch angular velocity ω_i through the equation $\dot{l}_i = r_w \omega_i$. Upon combining this relation with equation (7), one obtains a mapping between motor speeds and cable uncoiling speeds. Extending this relation to the moving-platform Cartesian displacements is the topic of the following subsection.

3.2 Cable-Driven Parallel Robot

From the parametrisation of the CDPC shown in Fig. 2 recall that both $A_1B_1B_2A_2$ and $A_1B_1B_3A_3$ are parallelograms. Also, let us define the position of point A_i expressed in frame $\mathcal{F}_b$ as ${}^b\mathbf{a}_i$, the position of point B_i in frame $\mathcal{F}_p$ as ${}^p\mathbf{b}_i$, and the

rotation matrix taking a vector from frame $\mathcal{F}_b$ to frame $\mathcal{F}_p$ as ${}^b\mathbf{R}_p$.

3.2.1 Instantaneous Kinematics

The first step towards the kinematic modelling of the manipulator is to write its loop closure equations, i.e,

$$\overrightarrow{A_iB_i} = l_i\,\mathbf{u}_i = \overrightarrow{A_iO} + \overrightarrow{OP} + \overrightarrow{PB_i} = -{}^b\mathbf{a}_i + {}^b\mathbf{p} + {}^b\mathbf{R}_p\,{}^p\mathbf{b}_i, \tag{8}$$

with $i = 1,2,3,4$.

The cable loop $A_3B_3B_2A_2$ is used to control both the length of the virtual cable $A_{32}B_{32}$ and the rotations of the embedded mechanism. By differentiation of Eq. (8), we obtain

$$\dot{l}_i\,\mathbf{u}_i + l_i\,\frac{d\mathbf{u}_i}{dt} = {}^b\dot{\mathbf{p}} + \frac{d^b\mathbf{b}_i}{dt} - \frac{d^b\mathbf{a}_i}{dt}, \tag{9}$$

$$\dot{l}_i\,\mathbf{u}_i + l_i\,\dot{\beta}_i\,\mathbf{E}\,\mathbf{u}_i = {}^b\dot{\mathbf{p}} + \dot{\varphi}\,\mathbf{E}\,{}^b\mathbf{b}_i, \tag{10}$$

where $d^b\mathbf{a}_i/dt = 0$ because $\mathbf{a}_i$ is constant in $\mathcal{F}_b$,

$$\mathbf{E} = \begin{bmatrix} 0 & -1 \\ 1 & 0 \end{bmatrix} \text{ and } {}^b\mathbf{b}_i = {}^b\mathbf{R}_p\,{}^p\mathbf{b}_i. \tag{11}$$

With $\varphi = 0^\circ$, the orientation of the MP,

$$\dot{l}_i\,\mathbf{u}_i + l_i\,\dot{\beta}_i\,\mathbf{E}\,\mathbf{u}_i = {}^b\dot{\mathbf{p}} + \dot{\varphi}\,\mathbf{E}\,{}^b\mathbf{R}_p\,{}^p\mathbf{b}_i \tag{12}$$

where $\dot{\beta}_i$ is the angular velocity of cable i in the fixed frame $\mathcal{F}_b$. In order to eliminate this passive variable, we multiply the Eq. (12) by $\mathbf{u}_i^T$:

$$\dot{l}_i\ \mathbf{u}_i^T\ \mathbf{u}_i + l_i\ \dot{\alpha}_i\ \mathbf{u}_i^T\ \mathbf{E}\ \mathbf{u}_i = \mathbf{u}_i^T\ {}^b\dot{\mathbf{p}} + \dot{\varphi}\ \mathbf{u}_i^T\ \mathbf{E}\ {}^b\mathbf{R}_p\ {}^p\mathbf{b}_i \tag{13}$$

The result can be written in matrix form :

$$\mathbf{A}\ \mathbf{t} = \mathbf{B}\ \dot{\mathbf{l}}, \tag{14}$$

where

$$\mathbf{A} = \begin{bmatrix} \mathbf{u}_1^T & \mathbf{u}_1^T\ \mathbf{E}\ {}^b\mathbf{b}_1 \\ \mathbf{u}_{32}^T & \mathbf{u}_{32}^T\ \mathbf{E}\ {}^b\mathbf{b}_{32} \\ \mathbf{u}_4^T & \mathbf{u}_4^T\ \mathbf{E}\ {}^b\mathbf{b}_4 \end{bmatrix},\ \mathbf{t} = \begin{bmatrix} \dot{\mathbf{p}} \\ \dot{\varphi} \end{bmatrix},\ \mathbf{B} = \mathbf{I}_3 \text{ and } \dot{\mathbf{l}} = \begin{bmatrix} \dot{l}_1 \\ \dot{l}_{32} \\ \dot{l}_4 \end{bmatrix}.$$

Assuming that the embedded pulley has a radius r_p, we obtain

$$\omega_p = \frac{\dot{l}_3 - \dot{l}_2}{2r_p}. \tag{15}$$

This leads to the overall Jacobian matrices :

$$\mathbf{A}_g\ \mathbf{t}_g = \mathbf{B}_g\ \dot{\mathbf{l}}_g \tag{16}$$

with,

$$\mathbf{A}_g = \begin{bmatrix} \mathbf{u}_1^T & \mathbf{u}_1^T\ \mathbf{E}\ {}^b\mathbf{b}_1 & 0 \\ \mathbf{u}_{32}^T & \mathbf{u}_{32}^T\ \mathbf{E}\ {}^b\mathbf{b}_{32} & 0 \\ \mathbf{u}_4^T & \mathbf{u}_4^T\ \mathbf{E}\ {}^b\mathbf{b}_4 & 0 \\ \mathbf{0}_2^T & 0 & 1 \end{bmatrix},\ \mathbf{t}_g = \begin{bmatrix} \dot{\mathbf{p}} \\ \dot{\varphi} \\ \dot{\alpha} \end{bmatrix}, \tag{17}$$

$$\mathbf{B}_g = \begin{bmatrix} 1 & 0 & 0 & 0 \\ 0 & \frac{1}{2} & \frac{1}{2} & 0 \\ 0 & 0 & 0 & 1 \\ 0 & -\frac{1}{2\ r_p} & \frac{1}{2\ r_p} & 0 \end{bmatrix},\quad \dot{\mathbf{l}}_g = \begin{bmatrix} \dot{l}_1 \\ \dot{l}_2 \\ \dot{l}_3 \\ \dot{l}_4 \end{bmatrix}, \tag{18}$$

where $\mathbf{A}_g \in \mathbb{R}^{4\times4}$ and $\mathbf{B}_g \in \mathbb{R}^{4\times4}$. Thus, if one needs to compute the cable uncoiling speeds from a prescribed twist of the end-effector, he or she can readily solve equation (16) as $\dot{\mathbf{l}} = \mathbf{J}_m\ \mathbf{t}$, where $\mathbf{J}_m = \mathbf{B}_g^{-1}\ \mathbf{A}_g$.

3.2.2 Static equilibrium

From the the application of the principle of virtual work to equation (16), we obtain

$$\mathbf{W}\ \boldsymbol{\tau} + \mathbf{w}_{ext} = \mathbf{0}_4, \tag{19}$$

with

$$\mathbf{W} = -\mathbf{J}_m^T = -\mathbf{A}_g^T\ \mathbf{B}_g^{-T}, \tag{20}$$

where $\mathbf{W} \in \mathbb{R}^{4\times4}$ is the wrench matrix of the manipulator, $\boldsymbol{\tau} = [\tau_1\ \cdots\ \tau_4]^T$ is the array of cable tensions, and $\mathbf{w}_{ext} = [0\ \ -mg\ 0\ m_E]^T$ is the external wrench applied on the end effector. The cable tension vector $\boldsymbol{\tau}$ can be obtained from the inverse of the wrench matrix $\mathbf{W}$ as long as it is not rank-deficient, namely, $\det(\mathbf{W}) \neq 0$.

$$\boldsymbol{\tau} = -\mathbf{W}^{-1}\mathbf{w}_{ext}. \tag{21}$$

From equation (7) and the principle of virtual work, the motor torques can be obtained as functions of the cable tensions. Let $\boldsymbol{\gamma}_M = [\gamma_A\ \gamma_B]^T$ be the two-dimensional vector containing the torques applied by the two motors of the transmission and $\boldsymbol{\tau}_E = [\tau_1\ \tau_2\ \tau_3]^T$, the three-dimensional vector containing the moments applied by the transmission to the three winchs 1, 2 and 3. From the principle of virtual work, the input work amounts to the output work as long as there is no loss in the transmission system. As a consequence,

$$\boldsymbol{\gamma}_M^T\ \boldsymbol{\omega}_M = \boldsymbol{\tau}_E^T\ \boldsymbol{\omega}_E \tag{22}$$

$$\boldsymbol{\gamma}_M^T\ \boldsymbol{\omega}_M = \boldsymbol{\tau}_E^T\ \mathbf{J}_D\ \boldsymbol{\omega}_M \tag{23}$$

Finally, the motor torques are expressed as a function of the moments exerted on the first three winchs as follows:

$$\gamma_M = \mathbf{J}_D^T \, \tau_E \tag{24}$$

3.2.3 Inverse Kinematics

The inverse kinematics of the CDPR itself is a simple matter. Indeed, from Fig. 12, when the position of point P on the moving platform is known, so are the positions of points B_i, $i = 1,\ldots,4$, and the cable lengths are directly computed as $l_i = \|\overrightarrow{A_iB_i}\|_2$, $i = 1,\ldots,4$. The winch angular positions $\theta_i(t)$, $i = 1,\ldots,4$, are computed by dividing the cable lengths by the corresponding winch radii.

Thence, we can find the the position angles of the output shaft of system {motor+ gearhead} at time t in rad, as :

$$\theta_1(t) = \frac{1}{2}[(\theta_A(t) - \theta_A(0)) + (\theta_B(t) - \theta_B(0))] + C \tag{25a}$$

$$\theta_2(t) = \theta_A(t) - \theta_A(0) \tag{25b}$$

$$\theta_3(t) = \theta_B(t) - \theta_B(0) \tag{25c}$$

We can assume that $\theta_A(0) = \theta_B(0) = 0$, which yields $C = \theta_1(0)$. With the mathematical relationships derived in this section, we are equipped to control the motion of the proposed robot and to determine its workspace, which is the topic of the following section.

3.2.4 Forward Kinematics

The forward kinematics of the transmission system is directly given by eq. (25). The cable lengths l_i, $i = 1,\ldots,4$, follow directly by multiplying the winch angles θ_i, $i = 1,\ldots,4$, with the corresponding winch radii. The angle of the embedded pulley can the be computed as

$$\theta_p = (l_3 - l_2)/r_p. \tag{26}$$

From Fig. 12, the position of point P is easily computed by considering the triangle with edges l_1, l_4 and $\overline{A_1A_4} + \overline{B_1B_4}$. Since the lengths of its three edges are known, it is a simple matter to compute the (x_b, y_b) coordinates of its apex in the base frame $\mathcal{F}_b$. This, in turn, directly yields the position of point P.

4 Workspace Analysis

This section consists of an analysis of the CDPC workspace and of the search of a cable layout that maximizes its size. The moving platform is in equilibrium for every possible external force-moment system $\mathbf{w}_{ext}$ if and only if, in every case, the Newton-Euler equilibrium, Eq. (19), can be satisfied by a set of feasible cable tensions $\boldsymbol{\tau}$. Such a pose of "complete" equilibrium of the moving-platform and of the embedded pulley is called a "feasible pose". The set of all feasible poses is called the "wrench-feasible workspace $\mathcal{F}$" and is formally expressed as follows,

$$\mathcal{F} = \{(\mathbf{p}, \phi, \alpha) \in \mathbb{R}^2 \times \mathbb{R} \times \mathbb{R} : \forall \mathbf{w}_{ext} \in \mathcal{W}_e, \exists \boldsymbol{\tau} \in \mathcal{T}, \mathbf{W}\,\boldsymbol{\tau} + \mathbf{w}_{ext} = \mathbf{0}_4\}, \tag{27}$$

where $\mathcal{W}_e$ is the set of external wrenches that can be applied on the moving-platform, including the moment exerted on the embedded pulley. $\mathcal{T}$ is the available cable tension set, which is a function of the available motor torques and of the Jacobian matrix $\mathbf{J}_D$ defined in Eq. (6).

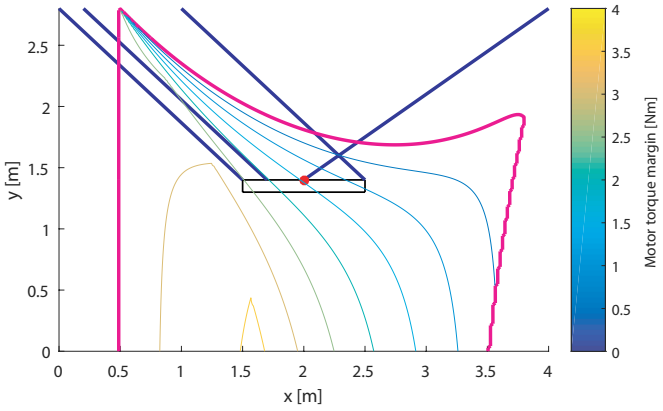

Fig. 6: Wrench feasible workspace of the planar CDPC with $m = 9$ kg and -1 Nm $\leq m_E \leq 1$ Nm

Figure 6 shows the boundary of the wrench feasible workspace $\mathcal{F}$ of the planar CDPC with a moving-platform weighing 9 kg and a moment m_E exerted on the embedded pulley and within the interval $[-1, 1]$ Nm. The isocontours of the motor torque margin are also traced in Fig. 6. The larger this margin, the higher the capability of the four motors to support the required torques. The Video 1[1] shows the evolution of $\mathcal{F}$ as a function of the mass m of the moving-platform and the upper bound $\overline{m}_E$ on the absolute value of the moment applied on the embedded pulley. It also shows the isocontours of the motor torque margin within $\mathcal{F}$.

[1] Video 1

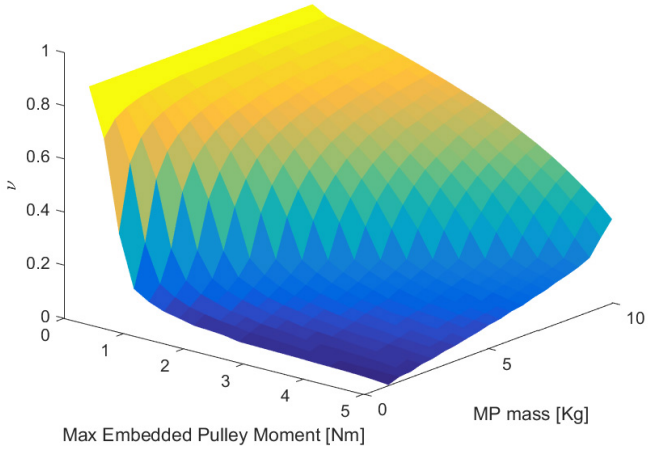

Fig. 7: Ratio ν between the areas of the WFW and the surface occupied by the robot in the vertical plane as a function of the MP mass and the maximum moment exerted on the embedded pulley

Let ν be the ratio between the areas of $\mathcal{F}$ and the surface occupied by the CDPC. Figure 7 shows this ratio as a function of m and $\overline{m}_E$ for a given cable layout. It is noteworthy that ν decreases as $\overline{m}_E$ increases. On the contrary, the larger m, the higher ν.

Figures (8a) to (8e) represent the evolution of the CDPC workspace according to the location of cable exit point B_4 on the moving-platform with $m = 8$ kg and $\overline{m}_E = 1\ Nm$. $\alpha_{xB4} = -1$ ($\alpha_{xB4} = 0$, $\alpha_{xB4} = 1$, respectively) means that B_4 is located at the left end (the middle, the right end, respectively) of the moving-platform. Interestingly, the workspace size is maximum when B_4 is in the middle of the moving-platform.

Figure 9 shows the ratio ν as a function of the moving-platform length and the location of point B_4, i.e., α_{xB4}. Besides, Video 2[2] shows the evolution of $\mathcal{F}$ according to the moving-platform length and α_{xB4}. No matter the length of the moving-platform, ν is maximum when α_{xB4} is null. Therefore, cable exit point B_4 is chosen to be the midpoint of the moving-platform in the CDPC prototype described in the following section.

5 Prototyping and Experimentation

In this section, we present an embodiment of the proposed concept and two test trajectories: one where pure translations and pure rotations are performed in sequence, and the other where they are combined in a generic motion.

[2] Video 2

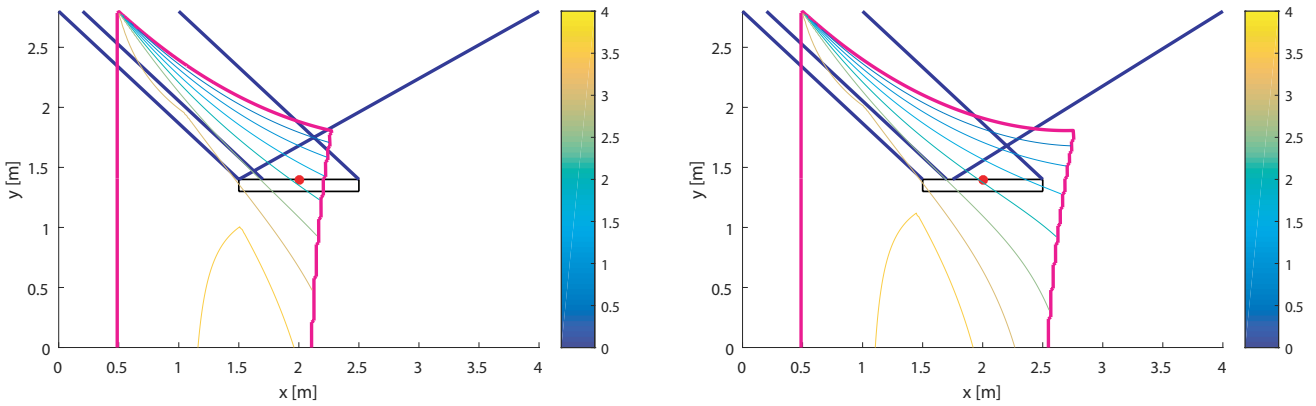

(a) $\alpha_{xB4} = -1$

(b) $\alpha_{xB4} = -0.5$

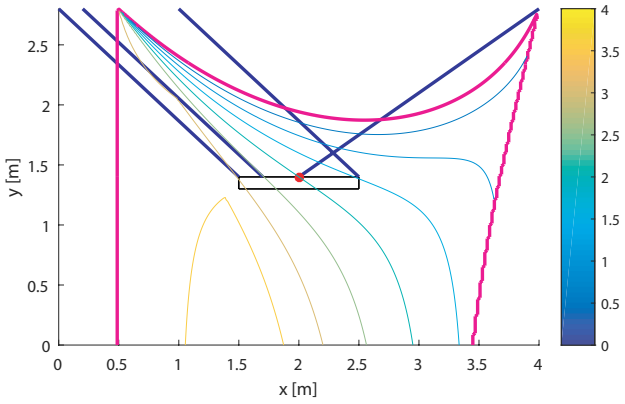

(c) $\alpha_{xB4} = 0$

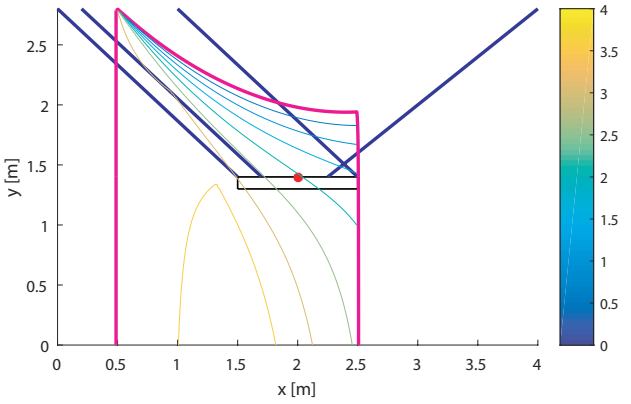

(d) $\alpha_{xB4} = 0.5$

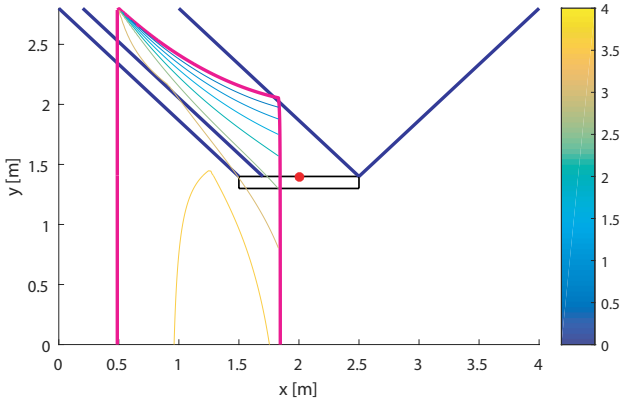

(e) $\alpha_{xB4} = 1$

Fig. 8: Wrench feasible workspace of the planar CDPC as a function of the location of the cable exit point B_4 with $m = 8$ kg and -1 Nm $\leq m_E \leq 1$ Nm

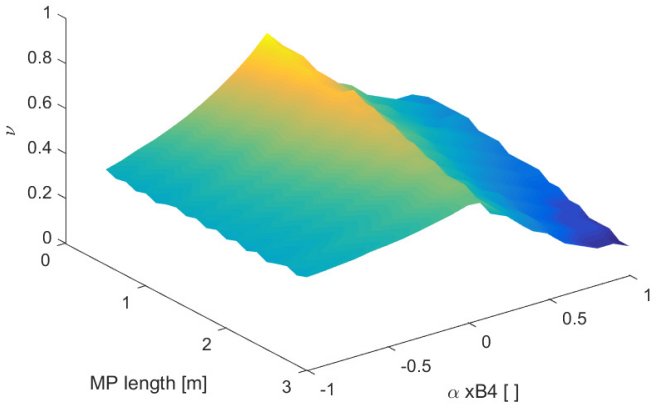

Fig. 9: Ratio ν between the WFW and the surface area occupied by the robot as a function of the MP length and the location of the cable exit point B_4 with $m = 9$ kg and -1 Nm $\leq m_E \leq 1$ Nm

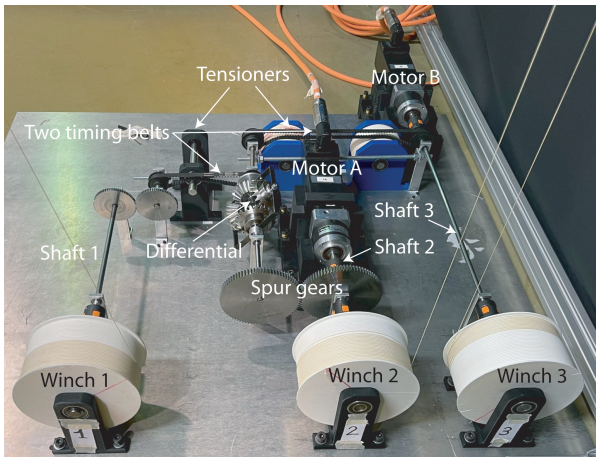

Fig. 10: Photograph of the Transmission system

5.1 Prototype presentation

The experimental demonstrator of the manipulator is manufactured as shown in Figs. 1 and 10. The architecture of the CDPC is presented in Fig. 13. The main hardware of the CREATOR demonstrator is shown in Fig. 11 and consists of a PC (equipped with ©MATLAB and ©ControlDesk software), a controller, a motor driver, winch assemblies, each comprising a servomotor, a gearbox and a drum and a moving platform. This testbed enables us to evaluate the capabilities of the proposed manipulator in operation.

This remainder of this section explains the experimental process followed to verify the viability of the concept. In particular, we wish to verify how susceptible it is to parasitic tilts by comparison with a previous design that did not involve

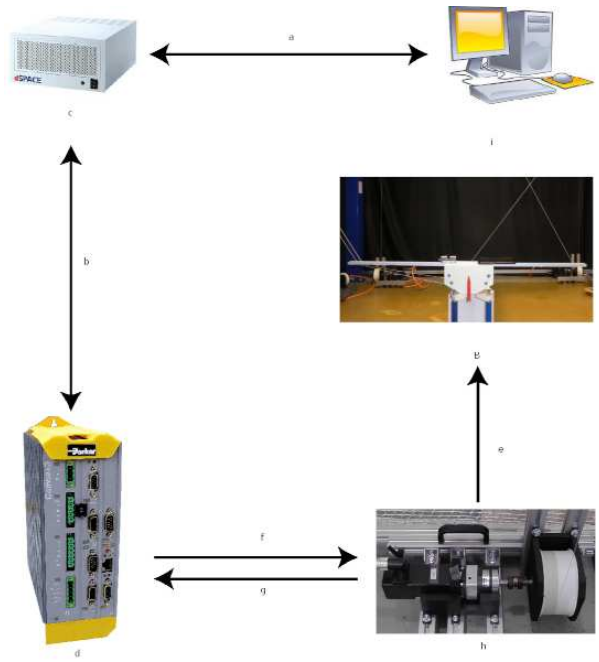

Fig. 11: Control architecture of the manipulator

a parallelogram. Firstly, the trajectories are defined in subsection 5.3. Then, the experiments 1 and 2 are described and discussed in sections 5.3.1 and 5.3.2, respectively.

5.2 Configurations

The goal of these experiments is to assess the effectiveness of the proposed architecture in preventing the parasitic tilts generated when applying moments through a cable loop. We do this by comparing the behaviour of our double-parallelogram configuration with that of a previous architecture without parallelogram or differential transmission. This reference configuration is presented in [19], and may be described as an under-constrained CDPR with three cables, three actuators and four dof. We call it $\mathcal{C}_1$. The configuration proposed in this article is shown in Fig. 2, and is a fully-actuated configuration with four cables, three actuators and three dof. We call it $\mathcal{C}_2$. These two configurations are shown in Figs. 13 (a) and (b), respectively.

5.3 Trajectories

Two trajectories were chosen in order to evaluate the performance of the parallelogram with respect to the platform orientation. One trajectory consists in moving separately the translation and rotation DoF of the inner mechanism; The other trajectory is a combination of these two motions. A polynomial of order five was used to define the trajectories.

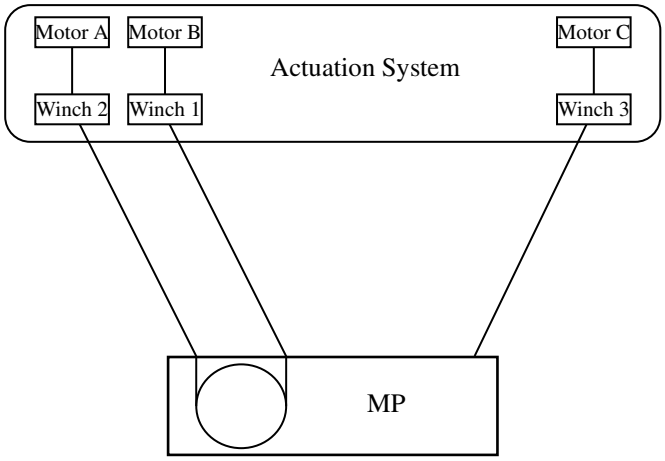

(a) Concept schematic of the three-cable configuration

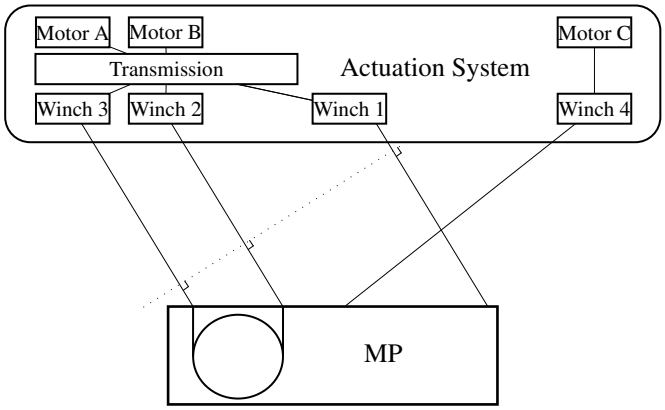

(b) Concept schematic of the four-cable configuration

Fig. 12: Schematics of the two robot configurations under study

5.3.1 Trajectory 1 - Pure Translations and Rotations in Sequence

The first trajectory, shown in Fig. 14, is a succession of translations and embedded-mechanism rotations. It may be described step by step as follows:

(a) Vertical translation from the stand P_0 to the position above the stand P_1 (33 s $\leq t \leq$ 43 s)

(b) Diagonal translation from P_1 to P_2 (43 s $\leq t \leq$ 53 s)

(c) Rotation anticlockwise of the embedded mechanism at P_2 (55 s $\leq t \leq$ 65 s)

(d) Rotation clockwise of the embedded mechanism at P_2 (63 s $\leq t \leq$ 73 s)

(e) Horizontal translation from P_2 to P_3 (73 s $\leq t \leq$ 93 s)

(f) Rotation anticlockwise of the embedded mechanism at P_3 (93 s $\leq t \leq$ 103 s)

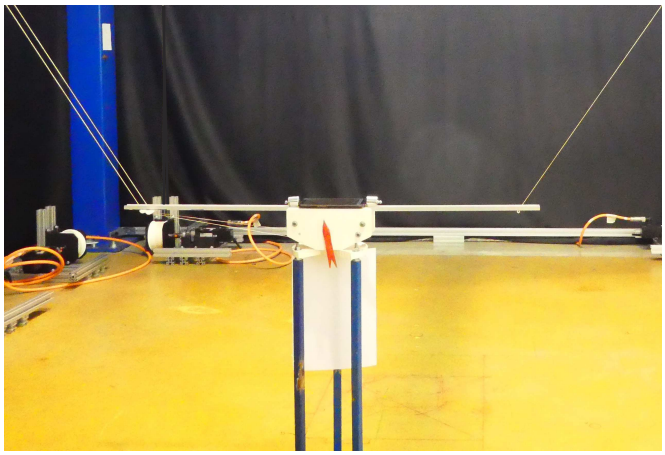

(a) Photograph of the three-cable configuration

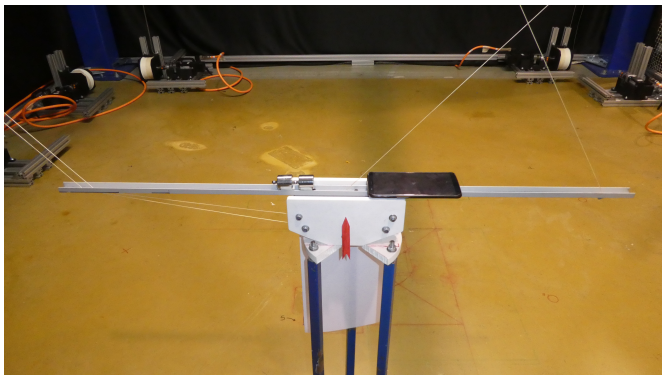

(b) Photograph of the four-cable configuration

Fig. 13: The two robot configurations

(g) Rotation clockwise of the embedded mechanism at P_3 (103 s $\leq t \leq$ 113 s)

(h) Diagonal translation from P_3 to P_1 (113 s $\leq t \leq$ 123 s)

(i) Vertical translation from above stand P_1 to stand position (123 s $\leq t \leq$ 133 s)

Point O being the origin of frame $\mathcal{F}_b$, the Cartesian coordinates of the control points of the Trajectory 1 are $\overrightarrow{OP_0} = [1.646\ 0.691]^T$ m, $\overrightarrow{OP_1} = [1.646\ 0.841]^T$ m, $\overrightarrow{OP_2} = [1\ 1]^T$ m, and $\overrightarrow{OP_3} = [2.5\ 1]^T$ m.

5.3.2 Trajectory 2 - Combined Translations and Rotations

The second trajectory is a combined movement of translation and cable loop rotation at the same time as presented in Fig. 15. The steps :

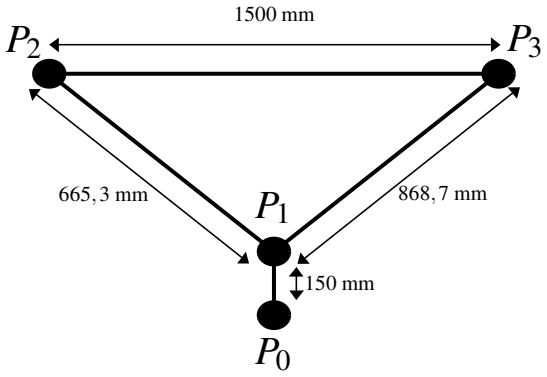

Fig. 14: Path of Trajectory 1 - pure translations and rotations in sequence

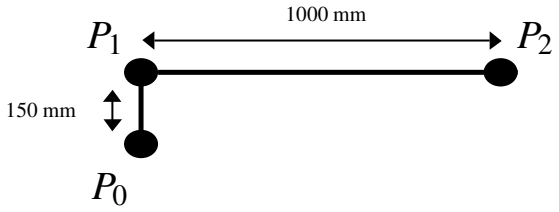

Fig. 15: Path of the Trajectory 2 - combined translations and rotations

(a) Vertical translation from the stand to the position P_1 above it (15 s $\leq t \leq$ 25 s)

(b) Rotation anticlockwise of the embedded mechanism at position P_1 above the stand (25 s $\leq t \leq$ 35 s)

(c) Horizontal translation while the embedded mechanism rotates clockwise from P_1 to P_2 (35 s $\leq t \leq$ 65 s)

The coordinates of the Trajectory 2 control points are $\overrightarrow{OP_1} = [1.646\ 0.691]^T$ m, $\overrightarrow{OP_2} = [2.646\ 0.691]^T$ m.

6 Result Analysis

The experiment consists in testing the two trajectories with the three-cable configuration and then with the four-cable configuration described in Fig. 13. During the experiment illustrated in Video3[3], the orientation around axis z_b was measured with an inclinometer on a phone to evaluate the system ability to stabilize the platform. Counterweights were used to statically balance the platform and thus cancel the weight of the phone. Also, the inner mechanism was represented by a red arrow.

[3] Video3

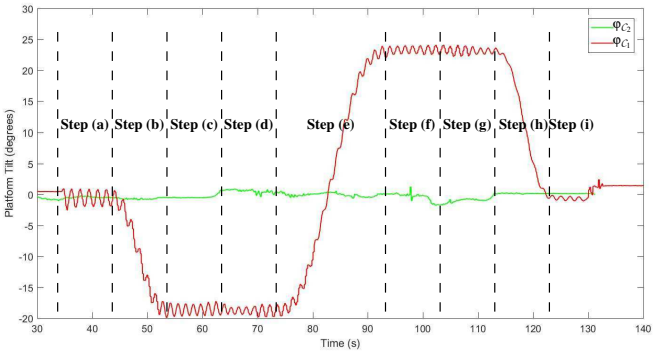

Fig. 16: Tilt angle around axis z_b - Trajectory 1

6.1 Description of the Results - Trajectory 1

Results of the experiments are shown in Figs. 16 and 17. The green curves describe the parasitic tilt ϕ of the four-cable configuration angle in degrees around axis z_b of the mobile platform. The red curves represent the same angle for the three-cable configuration.

In the first trajectory, the z_b rotation angle for the three-cable configuration decreases during step (b), reaches a mean of -18° during steps (c) and (d)increases at step (e). To stabilizes around 23° degrees at steps (f) and (g) and decreases back to 0° at step (h). A damped oscillation of the platform around axis z_b is visible during the whole experiment; its period is 1.6 s and its total amplitude starts at around 3°. The z_b rotation angle for the four-cable configuration is continuous and remains around 0° degree with approximately 1° of error during the whole test with no visible sign of oscillations.

6.2 Description of the Results - Trajectory 2

In the second trajectory, the z_b rotation angle for the three-cable configuration is continuous around 0° during steps (a) and (b) and increases to 27° during step (c). As in trajectory 1, oscillations of the moving platform can be observed by eye during the experiment. Angle measurements show that their oscillating period is 1.6 s and their amplitude is around 3.4°, figures that are closely similar to those obtained in trajectory 1. The z_b rotation angle for the four-cable configuration is continuous and remains around 0° with approximately 1° of error during the whole test with no sign of oscillations.

6.3 Discussion and Validation of the Results

The goal of this experiment was to demonstrate the effectiveness of the parallelogram cable structure. At the outset, we observe in both experiments that the three-cable configuration exhibits errors superior to 20° consistently increasing in

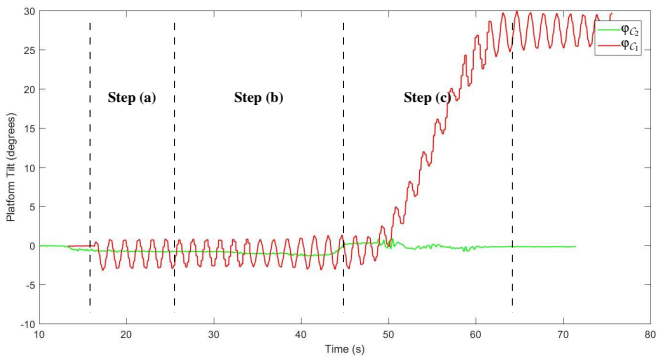

Fig. 17: Tilt angle around axis z_b - Trajectory 2

translation steps. We also have to consider the oscillations of the moving-platform in this configuration. Both of those errors may be attributed to the under-constrained nature of the robot. Indeed, this configuration has three motors and four DoFs, counting the translations in X and Y, the rotation about z_b and the inner DoF of the embedded mechanism.

The four-cable configuration is showing the expected results: a stable z_b angle with approximately 1° of error during the whole trajectory. Notice that a moving-platform starting with an offset angle would be bound to keep it during the entire experiment. What is important here is the continuity and stability of this angle.

The results obtained with both three- and four-cable configurations show the effectiveness of the parallelogram and validate the first hypothesis of this work. We can still observe in both trials that the 1° error appears in increments at step changes. For example, error increases can be seen in trajectory 1 between steps (c) and (d), (f) and (g) or at the end of step (c). These error changes seem to come from the overall transmission play and we can confidently assert that it is in large part an inversion play that occurs when the added winch 1 changes its direction of rotation.

6.4 Issues encountered and Solutions

The first tests for this experiment were met with mechanical issues. The first problem was the tooth jumps of the belts when the torque applied was too high caused by the insufficient belt tensions and the differential assembly being too flexible laterally. To avoid those jumps, the solutions was to add belt tensioners, to reinforce the in-between support tops with threaded rods and to reduce the weight. Unfortunately we were unable to remove the play inside the differential caused by an overly flexible satellite carrier. Likewise, we could not remove the plays in between tooths of the conical gears and in the flexible coupling.

At some point we decided to improve the stabilization by making the parallelogram wider in order to better demonstrate

the potential of our concept. Along the same line, we reduced the weight of the moving-platform by 3D-printing its frame and removing the embedded mechanism, replacing its hoist by a simple rotating arrow.

Concerning the cable loop, we can observe that the cable is slipping on the embedded mechanism during the experiment. Possible solutions would be to add weight on the platform to increase the cable tension or to make the drum surface more rough so as to increase friction.

During the tests, we also detected that the workspace was strongly impacted by the weight and the position of the 4th cable anchor point onto the mobile platform itself. It appears that positioning point B_4 in the middle of the platform, more precisely at mid-distance between B_1 and B_{32}, increases significantly the workspace of the robot as shown theoretically in Sec. 4.

7 Conclusions and Future Work

7.1 Conclusions

The main challenge of the article was to remove the unwanted rotations of the mobile platform of a planar CDPR with three actuators. The proposed solution was to add a cable to form a parallelogram capable of constraining the moving-platform rotations while keeping intact the cable loop system to activate the inner embedded mechanism and the number of motors. In order to achieve this challenge we designed a transmission module composed of a differential to control the added cable with the two motors on the left side of the robot. Finally, the experiments showed the viability and effectiveness of the solution proposed, as its rotation errors reached approximately 1°, compared to approximately 25° for the previously existing solution [19].

7.2 Future Work

As discussed in subsection 6.4, the first important point of improvement is to increase the stiffness of the transmission module, especially in the differential and belts. This point is vital for the accuracy of torque, position and speed of the added winch. More efficient tensioners and proper reinforcement of supports could be a solution. Furthermore, the play in-between teeth of the conical gears in the differential could be reduced by making a stiffer carrier and using helical conical gears. This application is a proof of concept and future work will consist in extending this concept to design a CDPR with a 3D workspace and capable of large rotations through cable loops.

Acknowledgements

This work was supported by the ANR CRAFT project, grant ANR-18-CE10-0004, https://anr.fr/Project-ANR-18-CE10-0004 and the RFI AtlanSTIC2020 CREATOR project.

Nomenclature

$\mathcal{F}_b(O_b, x_b, y_b, z_b)$ Frame attached to the robot base

$\mathcal{F}_p(O_p, x_p, y_p, z_p)$ Frame attached to the moving-platform

$\mathbf{l}_i$ i-th cable vector pointing from B_i to A_i, $i \in [\![1, \ldots, 4]\!]$

$\mathbf{a}_i$ Cartesian coordinates vector of point A_i, $i \in [\![1, \ldots, 4]\!]$

$\mathbf{b}_i$ Cartesian coordinates vector of point B_i, $i \in [\![1, \ldots, 4]\!]$

$\mathbf{p}$ Cartesian coordinates vector of point P

$\mathbf{u}_i$ i-th cable unit vector, $i \in [\![1, \ldots, 4]\!]$

$\mathbf{t}$ Cartesian parameter vector

$\mathbf{w}_e$ External wrench vector

$\boldsymbol{\tau}$ Cable tension vector

l_i i-th cable length, $i \in [\![1, \ldots, 4]\!]$

r_p Radius of the embedded pulley of the cable loop

A_i i-th cable exit point, $i \in [\![1, \ldots, 4]\!]$

B_i i-th cable anchor point, $i \in [\![1, \ldots, 4]\!]$

$\boldsymbol{\omega}_p$ Angular velocity of the embedded pulley

$\boldsymbol{\omega}_M$ Motor angular velocity vector

$\boldsymbol{\omega}_E$ Winch angular velocity vector

α Rotation angle of the embedded pulley

β_i Orientation angle of the ith cable

φ Tilt angle of the moving-platform

τ_i i-th cable tension

$\boldsymbol{\gamma}_M$ Torque applied on the moving-platform

${}^0\mathbf{R}_p$ Rotation matrix from frame $\mathcal{F}_b$ to frame $\mathcal{F}_p$

$\mathbf{W}$ Wrench matrix

$\mathbf{A}_g$ Forward Jacobian matrix of the robot

$\mathbf{B}_g$ Inverse Jacobian matrix of the robot

References

[1] Hussein, H., Santos, J. C., and Gouttefarde, M., 2018. "Geometric optimization of a large scale cdpr operating on a building facade". In 2018 IEEE/RSJ International Conference on Intelligent Robots and Systems (IROS), IEEE, pp. 5117–5124. 2

[2] Kawamura, S., Choe, W., Tanaka, S., and Pandian, S. R., 1995. "Development of an ultrahigh speed robot falcon using wire drive system". In Proceedings of 1995 IEEE International Conference on Robotics and Automation, IEEE, pp. 215–220. 2

[3] Gagliardini, L., Caro, S., Gouttefarde, M., and Girin, A., 2016. "Discrete reconfiguration planning for cable-driven parallel robots". *Mechanism and Machine Theory,* ***100***, pp. 313–337. PII: S0094114X16000513. 2

[4] Rasheed, T., Long, P., and Caro, S., 2020. "Wrench-feasible workspace of mobile cable-driven parallel robots". *Journal of Mechanisms and Robotics,* ***12***(3), Jan., p. 031009. 2

[5] Rasheed, T., Long, P., Roos, A. S., and Caro, S., 2019. "Optimization based Trajectory Planning of Mobile Cable-Driven Parallel Robots". In The 2019 IEEE/RSJ International Conference on Intelligent Robots and Systems (IROS 2019), pp. 6788–6793. 2

[6] Qian, S., Zi, B., Shang, W.-W., and Xu, Q.-S., 2018. "A review on cable-driven parallel robots". *Chinese Journal of Mechanical Engineering,* ***31***(1), p. 1007. PII: 267. 2

[7] Zake, Z., Chaumette, F., Pedemonte, N., and Caro, S., 2020. "Robust 2½d visual servoing of a cable-driven parallel robot thanks to trajectory tracking". *IEEE Robotics and Automation Letters,* ***5***(2), pp. 660–667. 2

[8] Bosscher, P., Williams, R. L., Bryson, L. S., and Castro-Lacouture, D., 2007. "Cable-suspended robotic contour crafting system". *Automation in Construction,* ***17***(1), pp. 45 – 55. 2

[9] Bostelman, R., Albus, J., Dagalakis, N., Jacoff, A., and Gross, J., 1994. "Applications of the nist robocrane". In Proceedings of the 5th International Symposium on Robotics and Manufacturing, Vol. 5. 2

[10] Blanchet, L., and Merlet, J.-P., 2014. "Interference detection for cable-driven parallel robots (cdprs)". In 2014 IEEE/ASME International Conference on Advanced Intelligent Mechatronics, pp. 1413–1418. 2

[11] Bak, J.-H., Hwang, S. W., Yoon, J., Park, J. H., and Park, J.-O., 2019. "Collision-free path planning of cable-driven parallel robots in cluttered environments". *Intelligent Service Robotics,* ***12***(3), pp. 243–253. PII: 278. 2

[12] Miermeister, P., and Pott, A., 2014. "Design of cable-driven parallel robots with multiple platforms and endless rotating axes". In *Interdisciplinary applications of kinematics*, A. Kecskeméthy and F. Geu Flores, eds., Vol. 26 of *Mechanisms and Machine Science*. Springer, pp. 21–29. 2

[13] Pott, A., and Miermeister, P., 2016. "Workspace and interference analysis of cable-driven parallel robots with an unlimited rotation axis". In Advances in Robot Kinematics, pp. 341–350. 2, 3

[14] Fortin-Côté, A., Faure, C., Bouyer, L., McFadyen, B. J., Mercier, C., Bonenfant, M., Laurendeau, D., Cardou, P., and Gosselin, C., 2017. "On the design of a novel cable-driven parallel robot capable of large rotation about one axis". In 3rd International Conference on Cable-Driven Parallel Robots, Springer, pp. 390–401. 2, 3

[15] Liu, H., Gosselin, C., and Laliberté, T., 2012. "Conceptual design and static analysis of novel planar spring-loaded cable-loop-driven parallel mechanisms". *Journal of Mechanisms and Robotics,* ***4***(2). 2

[16] Khakpour, H., and Birglen, L., 2014. "Workspace augmentation of spatial 3-dof cable parallel robots using differential actuation". In 2014 IEEE/RSJ International Conference on Intelligent Robots and Systems, IEEE, pp. 3880–3885. 2

[17] Khakpour, H., Birglen, L., and Tahan, S.-A., 2014. "Synthesis of differentially driven planar cable parallel manipulators". *IEEE Transactions on Robotics,* ***30***(3), pp. 619–630. 2

[18] Khakpour, H., Birglen, L., and Tahan, S.-A., 2015. "Analysis and optimization of a new differentially driven cable parallel robot". *Journal of Mechanisms and Robotics,* ***7***(3). 2

[19] Lessanibahri, S., Cardou, P., and Caro, S., 2018. "Kinetostatic analysis of a simple cable-driven parallel crane". In Volume 5A: 42nd Mechanisms and Robotics Conference, American Society of Mechanical Engineers. 2, 17, 23

[20] Longval, J. M., and Gosselin, C., 2019. "Dynamic trajectory planning and geometric analysis of a two-degree-of-freedom translational cable-suspended planar parallel robot using a parallelogram cable loop". *Journal of Mechanisms and Robotics,* ***11***(2). 4

[21] Lessanibahri, S., Cardou, P., and Caro, S., 2020. "A Cable-Driven Parallel Robot with an Embedded Tilt-Roll Wrist". *Journal of Mechanisms and Robotics,* ***12***(2), Feb. 4

[22] Métillon, M., Lessanibahri, S., Cardou, P., Subrin, K., and Caro, S., 2020. "A cable-driven parallel robot with full-circle end-effector rotations". In Volume 10: 44th Mechanisms and Robotics Conference (MR), American Society of Mechanical Engineers. 4

[23] Métillon, M., Cardou, P., Subrin, K., Charron, C., and Caro, S., 2021. "A Cable-Driven Parallel Robot with Full-Circle End-Effector Rotations". *Journal of Mechanisms and Robotics,* ***13***, June, pp. 031115–1 – 031115–9. 5, 27

List of Tables

List of Figures